ACS APPLIED POLYMER MATERIALS

pubs.acs.org/acsapm Article

Scalable Fabrication of Nano-Objects with Soft Polysiloxane Core and Functional Application as Toughening or Flame-Retardant Additives

Yu Hu, Jingwei Zhang, Hanyu Lv, Boyang Shi, Jiali Wu, Xiangcheng Pan,* and Guowei Wang*

Cite This: ACS Appl. Polym. Mater. 2026, 8, 2731−2745 Read Online

ACCESS | Metrics & More | Article Recommendations | Supporting Information

ABSTRACT: Polysiloxane has found extensive applications in advanced composite materials. However, the low compatibility with most polymers always resulted in the formation of macroscopic phase separation and thus limited its functional utilization to a maximum extent. Self-assembly of block copolymers has been developed as an efficient technique for preparing nanomaterials by selectively allocating each block at the core or shell region, thus facilitating multiple applications. However, the scalable fabrication and functional application of nano-objects with a soft polysiloxane core remain challenging, despite being boosted with theoretical significance and urgent applications. To this aim, herein, the poly(methyl methacrylate)-*b*-poly(dimethylsiloxane-*co*-vinylmethylsiloxane)-*b*-poly(methyl methacrylate) (PMMA-*b*-P(DMS-*co*-VMS)-*b*-PMMA, MSM) triblock copolymers were first designed and synthesized. Subsequently, employing a heat-induced self-assembly (HISA) process, the nano-objects with regular morphologies and controlled sizes were prepared in selective solvents and further stabilized by *in situ* cross-linking of the P(DMS-*co*-VMS) core. The observed low melting temperature (T_m) of the P(DMS-*co*-VMS) core confirmed that the soft polysiloxane core was successfully fabricated. The nano-objects with regular morphologies, controlled sizes, adjustable cross-linking densities, tunable PMMA contents, and block lengths significantly enhanced the toughening behavior and flame-retardant performance of PMMA-based composites, which were obviously superior to the counterpart of MSM triblock copolymer with undefined microphase. The HISA has proven to be an efficient technique for fabricating nano-objects with a soft polysiloxane core, which demonstrates significant potential as functional additives in practical applications.

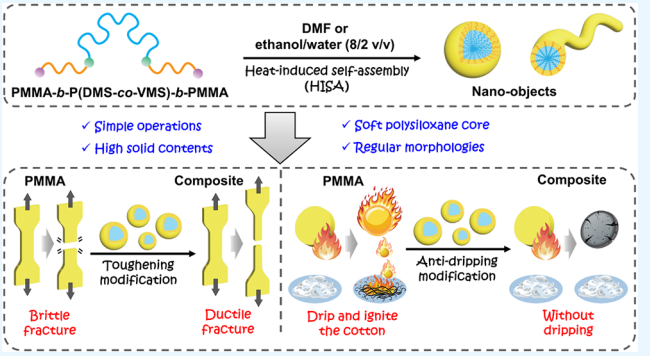

KEYWORDS: *polysiloxane, poly(methyl methacrylate), heat-induced self-assembly (HISA), toughening behavior, flame-retardant performance*

1. INTRODUCTION

Polysiloxane is a polymer with a main chain composed of alternating silicon and oxygen atoms with organic groups directly attached to the silicon atoms. This polymer exhibits unique flexibility, strong resistance to extreme temperatures, high hydrophobicity, intrinsic flame retardancy, and excellent physiological inertness, making it widely used in coatings, adhesives, electronics, medicine, flexible molding, care products, and so on.[1−3] For instance, the extremely low glass transition temperature (T_g) and unique flexibility of polysiloxane present significant potential for toughening applications, such as in epoxy resins and polymethacrylate.[4−6] Additionally, polysiloxane is widely used as a flame-retardant additive, eliminating the spread of fire caused by molten polymer droplets.[7,8] However, polysiloxane has low compatibility with most polymers, unavoidably leading to macroscopic phase separation or migration of polysiloxane to the surface, thereby hindering improvements in material performance. Efficiently incorporating the functional polysiloxane block into the composite nanomaterials is always a key issue.

Presently, using the powerful polymerization-induced self-assembly (PISA) process, the self-assembly of amphiphilic block copolymers (BCPs) in solution has greatly facilitated the preparation of nano-objects with various morphologies, including spherical, worm-like, and vesicular forms, by selectively allocating each block at the core or shell region.[9,10] Typically, these nano-objects have a core−shell structure, and the blocks in the core or shell regions play distinct and separate functions. Correspondingly, these nano-objects have been

Received: November 12, 2025
Revised: January 31, 2026
Accepted: February 1, 2026
Published: February 12, 2026

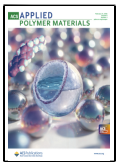

https://doi.org/10.1021/acsapm.5c04232
ACS Appl. Polym. Mater. 2026, 8, 2731−2745

Scheme 1. (a) Synthetic Route for MSM Triblock Copolymers and the Followed HISA Process. Illustration of (b) Toughening Modification and (c) Flame-Retardant Modification of the Prepared Nano-Objects

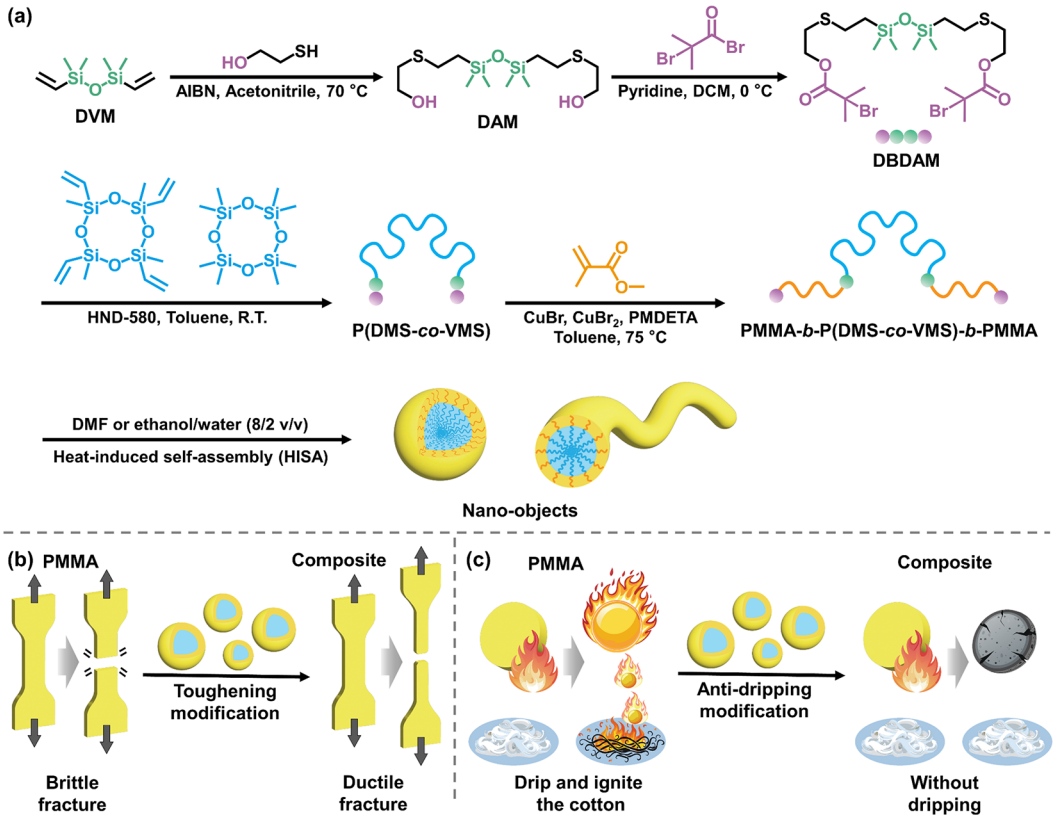

extensively developed as advanced nanomaterials and are involved in application fields such as composite nanomaterials, batteries, drug deliveries, sensors, catalysts, optoelectronics, and so on.[11−16] Following this conception, incorporating the polysiloxane into the shell or core regions of a nano-object becomes a solution to significantly improve the compatibility, as well as maximally elaborate the function of polysiloxane. However, up to now, the polysiloxane was dominantly designed as the shell in nano-objects, accompanied by a hard core with relatively high T_g, such as poly(benzyl methacrylate) (PBzMA), poly(2-hydroxypropyl methacrylate) (PHPMA), and poly(2-(dimethylamino)ethyl methacrylate) (PDMAEMA), and so on.[17−25] For example, using monocarbinol-terminated polydimethylsiloxane (PDMS) as a macromolecular chain transfer agent and 2-hydroxypropyl methacrylate (HPMA) as the monomer for the second block, Jennings et al. prepared nano-objects with PDMS as the shell by the PISA method at a solids content of 10% w/w.[17] Although nano-objects with a polysiloxane shell can be prepared at high solids content via the PISA method, this approach is not applicable to nano-objects with PDMS as the core. On the one hand, the challenge lies in the unique polymerization conditions for octamethylcyclotetrasiloxane (D_4) or related monomers. That is, no suitable solvent can meet the requirements for living ring-opening polymerization (ROP)-based PISA, in which the solvent should simultaneously act as a good solvent for the shell block and a poor solvent for the core block of polysiloxane. On the other hand, the challenge lies in the *in situ* stabilization of nano-objects with a soft polysiloxane core. Unlike the classical PISA process based on a core-forming block with a high T_g or melting temperature (T_m), the controlled cross-linking of the polysiloxane core should be performed *in situ*. Otherwise, the polysiloxane core with a low T_g or T_m tends to dissociate, and the already formed morphologies would be destroyed. Of course, it should be mentioned that nano-objects with polysiloxane as the core have been previously prepared by the conventional self-assembly strategy,[26−32] which is limited by low solids content (<1.0% w/w) and complicated operations. To the best of our knowledge, there are no reports on the preparation and application of nano-objects with a polysiloxane core at scalable high solids content (>5.0% w/w) and in a controlled manner, making this an ongoing challenge that requires urgent attention. Potentially, such nano-objects with a soft polysiloxane core are expected to have versatile applications, such as high-performance toughening agents or excellent flame-retardant additives.

Recently, our group proposed an efficient technique termed heat-induced self-assembly (HISA).[33] By adding presynthesized block copolymers or those combined with homopolymers into a selective solvent and employing a simple heating−cooling process, self-assembly occurs, resulting in the formation of nano-objects with different morphologies at high solids content. This technique offers advantages, such as simple operation, broad universality, and the absence of residual monomers and catalysts. However, the present HISA process only found limited success in the formation of nano-objects with a hard core, such as polystyrene (PS).

To expand the applicability of the HISA process, herein, the HISA process was tentatively employed to prepare nano-objects with a soft polysiloxane core from polysiloxane-based triblock copolymers, further aiming to develop advanced

https://doi.org/10.1021/acsapm.5c04232
ACS Appl. Polym. Mater. 2026, 8, 2731−2745

nanomaterials. In detail, we synthesized a difunctional compound of DBDAM, which contains a middle silicone linkage for the ring-opening polymerization (ROP) of cyclosiloxane monomers and two terminal bromide groups for the atom transfer radical polymerization (ATRP) of methyl methacrylate (MMA) monomers (Scheme 1). Subsequently, poly(methyl methacrylate)-*b*-poly(dimethylsiloxane-*co*-vinylmethylsiloxane)-*b*-poly(methyl methacrylate) (PMMA-*b*-P(DMS-*co*-VMS)-*b*-PMMA, labeled as MSM) triblock copolymers were prepared by sequential ROP and ATRP mechanisms. Using *N*,*N*-dimethylformamide (DMF) or an ethanol/water (8/2 v/v) mixture as selective solvents, the nano-objects with regular morphologies and controlled sizes were obtained via the HISA process, and the vinyl groups on VMS units in the core region were *in situ* cross-linked with ethanedithiol to stabilize the self-assembled structures. These nano-objects, with a P(DMS-*co*-VMS) core and a PMMA shell, exhibit soft-core characteristics and adjustable cross-linking densities. Due to the regular morphologies and controlled sizes, the function of the prepared nano-objects as toughening or flame-retardant agents was also explored, illustrating the important role of morphologies and sizes in the performance improvement of composites.

2. EXPERIMENTAL SECTION

2.1. Materials

Methyl methacrylate (MMA, 99%, Adamas) was passed through alkaline alumina to remove the inhibitor. Divinyl tetramethyl disiloxane (DVM, 98%, Guangzhou Hongcheng Biotechnology Co., Ltd.), 2-mercaptoethanol (98%, Macklin), ethanedithiol (EDT, 98%, Adamas), 2,2-azobis(2-methylpropionitrile) (AIBN, 98%, Adamas), 2-bromo-2-methylpropionyl bromide (BiBB, 98%, Adamas), pyridine (99.5%, Adamas), octamethylcyclotetrasiloxane (D_4, 98%, Jining Huakai Resin Co., Ltd.), 2,4,6,8-tetramethyl-2,4,6,8-tetravinylcyclotetrasiloxane (V_4, 98%, Guangzhou Yuanda New Materials Co., Ltd.), solid acid catalyst (HND-580, Jiangyin Nanda Synthetic Chemistry Co., Ltd.), cuprous bromide (CuBr, 99%, Adamas), cupric bromide ($CuBr_2$, 99%, Adamas), N,N,N′,*N*″,*N*‴-pentamethyldiethylenetriamine (PMDETA, 98%, Adamas), *N*,*N*-dimethylformamide (DMF, 99.5%, Sinopharm Chemical Reagent Co., Ltd. (SCRC)), toluene (99.5%, SCRC), ethanol (99.5%, SCRC), tetrahydrofuran (THF, 99.5%, SCRC), acetonitrile (99.5%, SCRC), dichloromethane (DCM, 99.9%, Adamas), and poly(methyl methacrylate) (PMMA 8817, Evonik Industries AG) were used as received. All other reagents were purchased from SCRC and used as received, except for an additional declaration.

2.2. Synthesis of DAM Precursor

First, the DVM (10.0136 g, 53.7 mmol), 2-mercaptoethanol (12.4859 g, 160 mmol), AIBN (0.9850 g, 6.00 mmol), and acetonitrile (100 mL) were sequentially added into a 250 mL round-bottom flask. Then, the nitrogen was charged for 30 min to exchange the oxygen, and the reaction was carried out at 70 °C. After 24 h, the solvent was removed by rotary evaporation, and the residue was dissolved in ethyl acetate (200 mL), followed by washing with deionized water (50 mL × 3) and saturated brine (50 mL × 3). The organic layer was dried with anhydrous sodium sulfate and concentrated by rotary evaporation. The purification was performed through column chromatography with petroleum ether/ethyl acetate (3/2 v/v), yielding a colorless liquid with a yield of 91%.

^{1}H NMR ($CDCl_3$, δ, ppm, TMS): 0.03 (s, 12H, −C***H***$_3$ on silicon), 0.78−0.87 (m, 4H, −Si$(CH_3)_2$−C***H***$_2$−), 2.49−2.56 (m, 4H, −S−C***H***$_2$−CH_2−Si$(CH_3)_2$−), 2.65−2.70 (t, 4H, −S−C***H***$_2$−CH_2−OH), 2.73−2.97 (s, 2H, −O***H***), 3.62−3.70 (t, 4H, −C***H***$_2$−OH). ^{13}C NMR ($CDCl_3$, δ, ppm, TMS): 0.40 (−***C***H_3 on silicon), 19.11 (−Si$(CH_3)_2$−***C***H_2−), 26.64 (−S−***C***H_2−CH_2−Si$(CH_3)_2$−), 34.88 (−S−***C***H_2−CH_2−OH), 60.43 (−***C***H_2−OH).

2.3. Synthesis of DBDAM Precursor

First, the DAM (5.0060 g, 14.6 mmol) and DCM (100 mL) were added into a 250 mL round-bottom flask. Then, the pyridine (4.6201 g, 58.4 mmol) and BiBB (10.0457 g, 43.7 mmol) were dropped into the flask under an ice water bath, and the reaction was carried out for 24 h. After the sediment was removed by suction filtration, the solution was washed with deionized water (50 mL × 3) and saturated brine (50 mL × 3). The organic layer was dried with anhydrous sodium sulfate and then concentrated by rotary evaporation. The purification was performed through column chromatography with petroleum ether/ethyl acetate (19/1 v/v), yielding a colorless liquid with a yield of 88%.

^{1}H NMR ($CDCl_3$, δ, ppm, TMS): 0.03 (s, 12H, −C***H***$_3$ on silicon), 0.82−0.92 (m, 4H, −Si$(CH_3)_2$−C***H***$_2$−), 1.89−1.95 (s, 12H, −C(C***H***$_3)_2$−Br), 2.49−2.56 (m, 4H, −S−C***H***$_2$−CH_2−Si$(CH_3)_2$−), 2.65−2.70 (t, 4H, −S−C***H***$_2$−CH_2−O−), 4.25−4.32 (t, 4H, −C***H***$_2$−O−). ^{13}C NMR ($CDCl_3$, δ, ppm, TMS): 0.51 (−***C***H_3 on silicon), 19.11 (−Si$(CH_3)_2$−***C***H_2−), 27.39 (−S−***C***H_2−CH_2−Si$(CH_3)_2$−), 30.01 (−S−***C***H_2−CH_2−O−), 30.84 (−C(***C***$H_3)_2$−Br), 55.72 (−***C***$(CH_3)_2$−Br), 65.09 (−***C***H_2−O−), 171.52 (−***C***OO−).

2.4. Synthesis of P(DMS-*co*-VMS) Precursor

The P(DMS-*co*-VMS) precursor is labeled as P(DMS-*co*-VMS)-x-y, where "x" represents the molecular weight (MW) of P(DMS-*co*-VMS), and "y" represents the molar fraction of VMS in P(DMS-*co*-VMS). Take the synthesis of P(DMS-*co*-VMS)-52.9k-13% as an example. First, DBDAM (0.4377 g, 0.683 mmol), D_4 (32.1149 g, 108 mmol), V_4 (8.0580 g, 23.4 mmol), HND-580 (4.0388 g), and toluene (46 mL) were sequentially added into a 250 mL round-bottom flask. The reaction was carried out at room temperature for 72 h. After the removal of HND-580 by suction filtration, the solvent was removed by rotary evaporation. Finally, the polymer was precipitated in methanol three times and dried in a vacuum oven.

P(DMS-*co*-VMS)-52.9k-13%, SEC: $M_{n,SEC}$ = 20 000 g/mol, M_w/M_n = 2.05. ^{1}H NMR ($CDCl_3$, δ, ppm, TMS): 0.02−0.20 (−C***H***$_3$ on silicon), 0.87−0.95 (m, −Si$(CH_3)_2$−C***H***$_2$−), 1.93−1.96 (s, −C(C***H***$_3)_2$−Br), 2.62−2.69 (m, −S−C***H***$_2$−CH_2−Si$(CH_3)_2$−), 2.77−2.83 (t, −S−C***H***$_2$−CH_2−O−), 4.28−4.35 (t, −C***H***$_2$−O−), 5.72−6.07 (—C***H***═C***H***$_2$ on silicon). ^{29}Si NMR ($CDCl_3$, δ, ppm, TMS): −36.0−34.9 (VMS unit), −22.1−20.8 (DMS unit).

2.5. Synthesis of PMMA-*b*-P(DMS-*co*-VMS)-*b*-PMMA (MSM) Triblock Copolymer

The MSM triblock copolymers are labeled as MSM-x-y-z, where "x" and "y" denote the same parameters as those in P(DMS-*co*-VMS), and "z" represents the mass fraction of PMMA in the MSM triblock copolymers. Take the synthesis of MSM-52.9k-13%-28% as an example. First, the P(DMS-*co*-VMS)-52.9k-13% (14.9840 g, 0.283 mmol), MMA (14.1450 g, 141 mmol), PMDETA (0.0981 g, 0.566 mmol), and toluene

https://doi.org/10.1021/acsapm.5c04232
ACS Appl. Polym. Mater. 2026, 8, 2731−2745

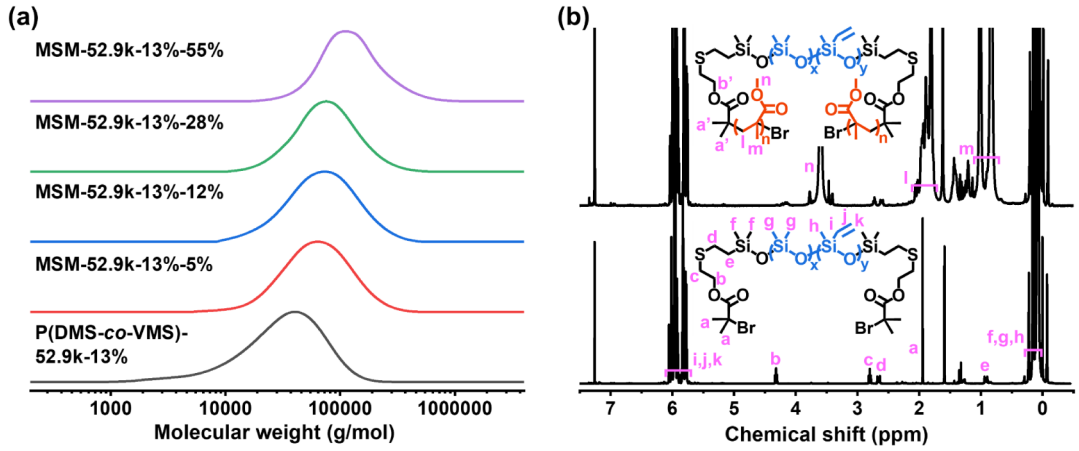

Figure 1. (a) SEC curves for P(DMS-*co*-VMS)-52.9k-13% and the corresponding MSM triblock copolymers. (b) ^{1}H NMR spectrum for P(DMS-*co*-VMS)-52.9k-13% and MSM-52.9k-13%-28% triblock copolymer (in $CDCl_3$).

(95 mL) were added into a 250 mL Schlenk flask, and the freezing-pumping-thawing cycle was repeated three times to remove the oxygen. After the third freeze, CuBr (0.0251 g, 0.175 mmol) and $CuBr_2$ (0.0258 g, 0.116 mmol) were added, and the reaction was carried out at 75 °C for 16 h. After the polymer was passed through neutral alumina to remove copper salts, the solvent was removed by rotary evaporation. Finally, the polymer was precipitated in methanol three times and dried in a vacuum oven.

MSM-52.9k-13%-28%, SEC: $M_{n,SEC}$ = 62 300 g/mol, M_w/M_n = 1.46. ^{1}H NMR ($CDCl_3$, δ, ppm, TMS): 0.02−0.20 (−C***H***$_3$ on silicone), 0.70−1.10 (≡C—C***H***$_3$ on PMMA), 1.69−2.08 (−C***H***$_2$− on PMMA), 3.48−3.75 (−OC***H***$_3$ on PMMA), 5.72−6.07 (—C***H***═C***H***$_2$ on silicone).

2.6. Preparation of Nano-Objects via HISA Process

Take the HISA process of MSM-52.9k-13%-28% triblock copolymer in DMF with a solids content of 10% w/w as an example. First, the MSM-52.9k-13%-28% (1.0065 g, 0.0137 mmol) and DMF (9.0044 g) were added and sealed into a 20 mL vial, stirred at 100 °C for 4 h, and then cooled to 70 °C. After the nitrogen was charged for 5 min to remove the oxygen, the AIBN (0.1565 g, 0.953 mmol) and EDT (0.0885 g, 0.939 mmol) were added into the flask. For complete consumption of the vinyl group and controlled cross-linking density, the molar amounts of AIBN and EDT are 1.5 times that of double bonds on P(DMS-*co*-VMS). After the nitrogen was charged for another 5 min, the reaction was carried out at 70 °C for 10 h. Finally, the nano-objects were precipitated in methanol three times and dried in a vacuum oven. Similarly, the HISA process was also performed in an ethanol/water (8/2, v/v) mixture.

2.7. Preparation of PMMA-Based Composite

The PMMA-based composite was prepared by mixing the above nano-objects with PMMA 8817 using a HAAKE MiniLAB3 (Thermo Fisher). The rotating speed and temperature were set at 50 rpm and 180 °C, respectively. After blending for 10 min in "Cycle" mode, the mixture was extruded and granulated. The samples for the impact test, tensile test, and combustion test were molded using a GT-7014-H30C flat vulcanizing machine (GOTECH, Taiwan) and steel molds under a pressure of 5 T at 180 °C.

Additional testing and characterization methods are detailed in the Supporting Information.

3. RESULTS AND DISCUSSION

3.1. Synthesis and Characterization of MSM Triblock Copolymers

To synthesize the targeted MSM triblock copolymers, a difunctional compound of DBDAM, containing a middle silicone linkage for the ROP of cyclosiloxane monomers and two terminal bromide groups for the ATRP of MMA monomers, was first prepared. In detail, the vinyl groups on DVM were first modified with 2-mercaptoethanol via an efficient thiol−ene reaction, and the DAM was obtained. Subsequently, the generated hydroxyl groups at the two terminal ends of DAM were modified with BiBB via an efficient esterification reaction, and DBDAM was thus collected. The structure of the obtained DBDAM was comprehensively characterized and confirmed by proton/carbon nuclear magnetic resonance (^{1}H NMR^{13}C NMR) spectra (Figure S1), respectively.

Furthermore, using DBDAM as the initiator, the solid acid (HND-580) catalyzed ROP of D_4 and V_4 was conducted to synthesize a random copolymer of dimethylsiloxane (DMS) and methyl vinyl siloxane (VMS), P(DMS-*co*-VMS). Typically, the ROP of cyclosiloxanes is accompanied by chain scission reactions, leading to an equilibrium between cyclic and linear siloxanes,[34,35] and thus leading to the random incorporation of DMS and VMS units into the middle of the DBDAM initiator. The SEC results showed that the equilibrium reaction of cyclosiloxane resulted in a relatively broad molecular weight distribution (MWD, M_w/M_n) for P(DMS-*co*-VMS) (Figure 1a, Figure S2). By variation of the feed molar ratio of DBDAM to D_4 and V_4 monomers, P(DMS-*co*-VMS) copolymers with different MWs and VMS unit contents were generated. The structure of the P(DMS-*co*-VMS) copolymers was also confirmed by ^{1}H NMR spectra (Figure 1b), indicating the typical resonance signals of protons (—C***H***═C***H***$_2$) at 5.72−6.07 ppm and methyl protons (−C***H***$_3$) at 0.02−0.20 ppm. According to the ^{1}H NMR spectra, the molar fractions of VMS units in P(DMS-*co*-VMS) were calculated to be 3%, 11%, 13%, and 36%, respectively. Meanwhile, the ^{29}Si NMR spectra of the P(DMS-*co*-VMS) copolymers revealed multiple sequence distributions of DMS and VMS units, rather than a sequence of four DMS units (from the D_4 monomer) or four VMS units (from the V_4 monomer) (Figure S3). This indicated that the cyclosiloxane was disrupted and rearranged during the acid-

https://doi.org/10.1021/acsapm.5c04232
ACS Appl. Polym. Mater. 2026, 8, 2731−2745

Table 1. Characterization Data for MSM Triblock Copolymers and the Corresponding Precursors

	P(DMS-*co*-VMS)		PMMA		MSM		
Sample	$M_{n,NMR}$ (g/mol)[a]	x_{VMS} (%)[b]	$M_{n,NMR}$ (g/mol)[a]	y_{PMMA} (%)[b]	$M_{n,NMR}$ (g/mol)[a]	$M_{n,SEC}$ (g/mol)[c]	M_w/M_n[c]
MSM-24.4k-36%-47%	24,400	36	21,400	47	45,800	47,600	1.51
MSM-24.4k-36%-27%	24,400	36	9,000	27	33,400	30,000	1.40
MSM-21.8k-11%-41%	21,800	11	14,900	41	36,700	35,000	1.43
MSM-21.8k-11%-28%	21,800	11	8,500	28	30,300	29,400	1.43
MSM-20.9k-3%-46%	20,900	3	18,000	46	38,900	36,000	1.36
MSM-20.9k-3%-26%	20,900	3	7,300	26	28,200	30,300	1.45
MSM-52.9k-13%-55%	52,900	13	65,300	55	118,200	102,600	1.45
MSM-52.9k-13%-28%	52,900	13	20,400	28	73,300	62,300	1.46
MSM-52.9k-13%-12%	52,900	13	7,100	12	60,000	53,900	1.60
MSM-52.9k-13%-5%	52,900	13	2,900	5	55,800	49,000	1.56

[a]$M_{n,NMR}$ was calculated according to the ^{1}H NMR spectra. [b]The molar fraction of VMS in P(DMS-*co*-VMS) and the mass fraction of PMMA in MSM triblock copolymer were calculated according to the ^{1}H NMR spectra. [c]$M_{n,SEC}$ and M_w/M_n were obtained by SEC measurement using THF as eluent and PMMA as standard.

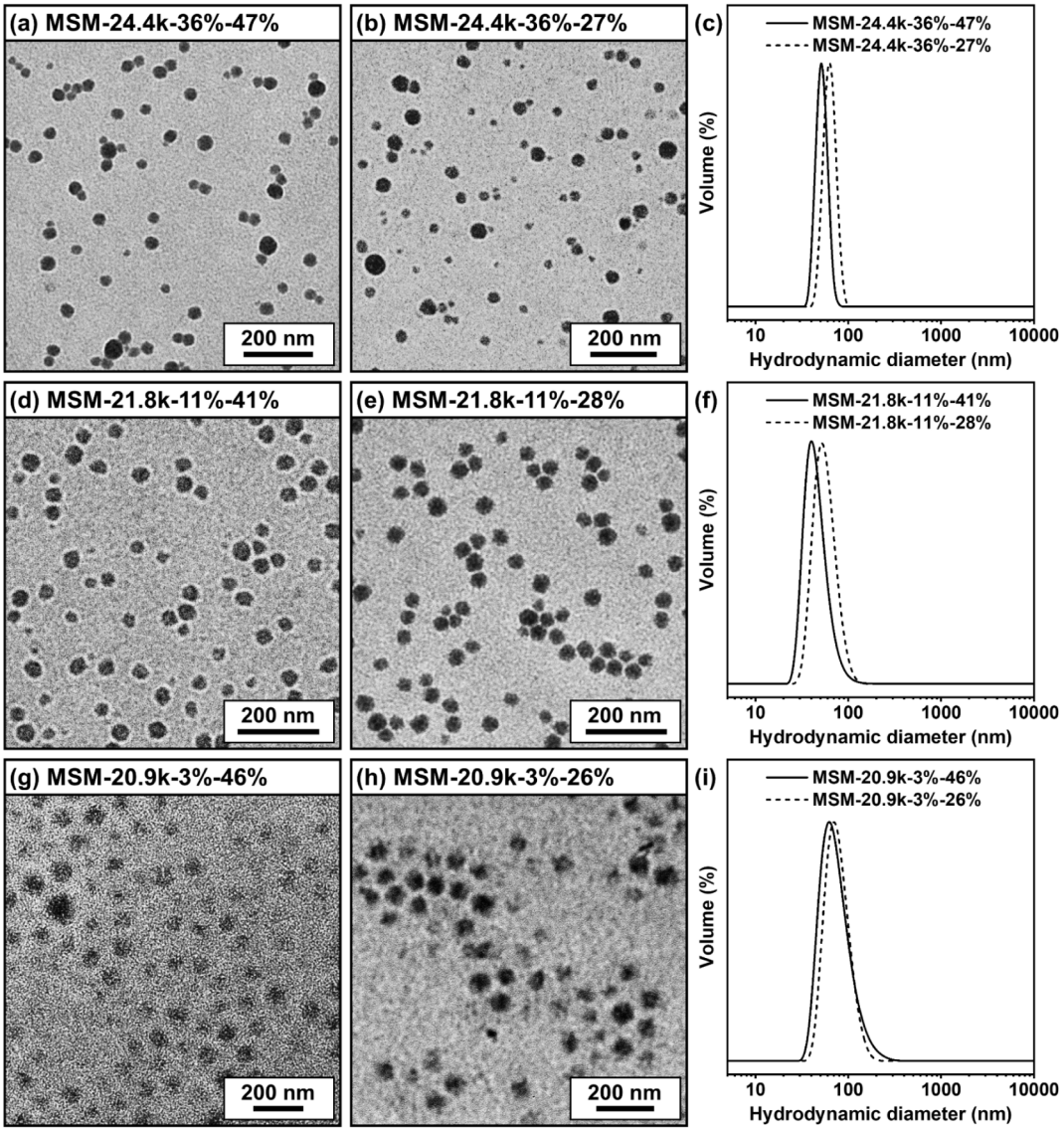

Figure 2. TEM images of nano-objects (diluted as 0.03% w/w dispersion in toluene) generated by HISA process in DMF with solids content of 10% w/w from (**a**) MSM-24.4k-36%-47%, (**b**) MSM-24.4k-36%-27%, (**d**) MSM-21.8k-11%-41%, (**e**) MSM-21.8k-11%-28%, (**g**) MSM-20.9k-3%-46%, and (**h**) MSM-20.9k-3%-26% triblock copolymers. (**c, f, i**) DLS results of the corresponding nano-objects in toluene.

catalyzed ROP process, leading to the formation of a random structure with DMS and VMS units, which was consistent with

https://doi.org/10.1021/acsapm.5c04232
ACS Appl. Polym. Mater. 2026, 8, 2731−2745

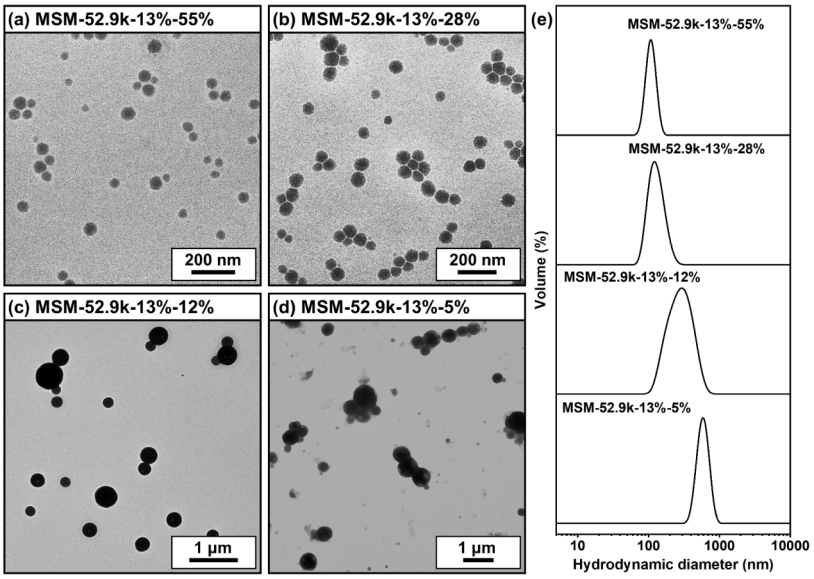

Figure 3. TEM images of nano-objects (diluted as 0.03−0.3% w/w dispersion in toluene) generated by HISA process in DMF with solids content of 10% w/w from (**a**) MSM-52.9k-13%-55%, (**b**) MSM-52.9k-13%-28%, (**c**) MSM-52.9k-13%-12%, and (**d**) MSM-52.9k-13%-5% triblock copolymers. (**e**) DLS results of the corresponding nano-objects in toluene.

reports in the literature.[36,37] The random structure would facilitate the formation of uniform cross-linking density in P(DMS-*co*-VMS) core during the following HISA process.

Finally, P(DMS-*co*-VMS) copolymers were used as macro-initiators to synthesize the targeted MSM triblock copolymers via the ATRP process. Comparatively, the SEC curves showed that the generated MSM triblock copolymers had relatively lower M_w/M_ns than the corresponding P(DMS-*co*-VMS) precursors (Figure 1a, Figure S2). The reason might be attributed to the controlled/"living" character of the ATRP mechanism,[38,39] which narrowed the M_w/M_n of the PMMA block and the corresponding MSM triblock copolymers. From the ^{1}H NMR spectrum (Figure 1b), the characteristic resonance signals attributed to the protons (CH_3O-) on the MMA unit were observed at 3.48−3.75 ppm, where some additional signals were overlapped and might be attributed to trace methanol introduced during the precipitation process. By modulation of the MW of P(DMS-*co*-VMS) and the feed molar ratio of P(DMS-*co*-VMS) to the MMA monomer, the MSM triblock copolymers with different MWs and PMMA block contents were synthesized (Table 1).

3.2. HISA Process of MSM Triblock Copolymers in Selective Solvent

Using the MSM triblock copolymers described above with different compositions as research models, the HISA process was investigated. As confirmed in our previous work,[33] the elevated temperatures facilitate the solvation and plasticization of the core-forming blocks, enabling the BCPs to undergo rearrangement in selective solvents. Subsequently, the cooling process induced the aggregation of BCPs into nano-objects. The morphological differences could be attributed to the common functions of solvents and temperatures, affecting the solubility of BCPs in selective solvents. For the MSM triblock copolymers, the polar solvent DMF is a good solvent for the PMMA block but a poor solvent for the P(DMS-*co*-VMS) block. Thus, using DMF as a selective solvent, the HISA process could be realized for the formation of nano-objects with a PMMA shell and a P(DMS-*co*-VMS) core. As the core-forming P(DMS-*co*-VMS) block has a composition and structure similar to that of PDMS or PVMS, it is expected to have a low T_g or T_m similar to those of PDMS (T_g around −120 °C, T_m around −50 °C) or PVMS (T_g around −100 °C).[40−42] Therefore, the nano-objects should be stabilized to maintain their self-assembled morphologies by cross-linking the P(DMS-*co*-VMS) block in the core region. That was also the reason why the VMS unit was introduced into the copolymers, which provided the reactive vinyl group with a controlled density. Herein, after the BCPs were heated and stirred at 100 °C, the system was cooled to 70 °C and charged with nitrogen. The following cross-linking reaction was achieved through a radical-mediated thiol−ene reaction between the vinyl groups on P(DMS-*co*-VMS) and EDT, in the presence of AIBN. For complete consumption of the vinyl group and controlled cross-linking density, the molar amounts of AIBN and EDT are 1.5 times that of the double bonds on P(DMS-*co*-VMS) block. Correspondingly, by varying the vinyl group content in P(DMS-*co*-VMS), the core's cross-linking density could be modulated. After the HISA process, the system was cooled to room temperature (25 °C), and the nano-objects were recovered by precipitation and redispersed into toluene, which was a good solvent for both the PMMA and P(DMS-*co*-VMS) blocks, for the transmission electron microscopy (TEM) measurements.

First, fixing the core-forming block as P(DMS-*co*-VMS)-20.9k-3%, P(DMS-*co*-VMS)-21.8k-11%, and P(DMS-*co*-VMS)-24.4k-36% with relatively lower MWs between 20 and 25k, as shown in Figure 2, spherical nano-objects were predominantly formed in DMF solvent with a solids content of 10% w/w. The nano-objects generated from MSM-20.9k-3%-46% and MSM-20.9k-3%-26% exhibited vague contours, while those from MSM-21.8k-11%-41%, MSM-21.8k-11%-28%, MSM-24.4k-36%-47%, and MSM-24.4k-36%-27% displayed relatively high contrast. This difference could be attributed to the lower VMS unit content and cross-linking density in the P(DMS-*co*-VMS) core in the former cases, which tended to form nano-objects with relatively loose structure. Additionally, the nano-objects formed from the MSM triblock copolymer

https://doi.org/10.1021/acsapm.5c04232
ACS Appl. Polym. Mater. 2026, 8, 2731−2745

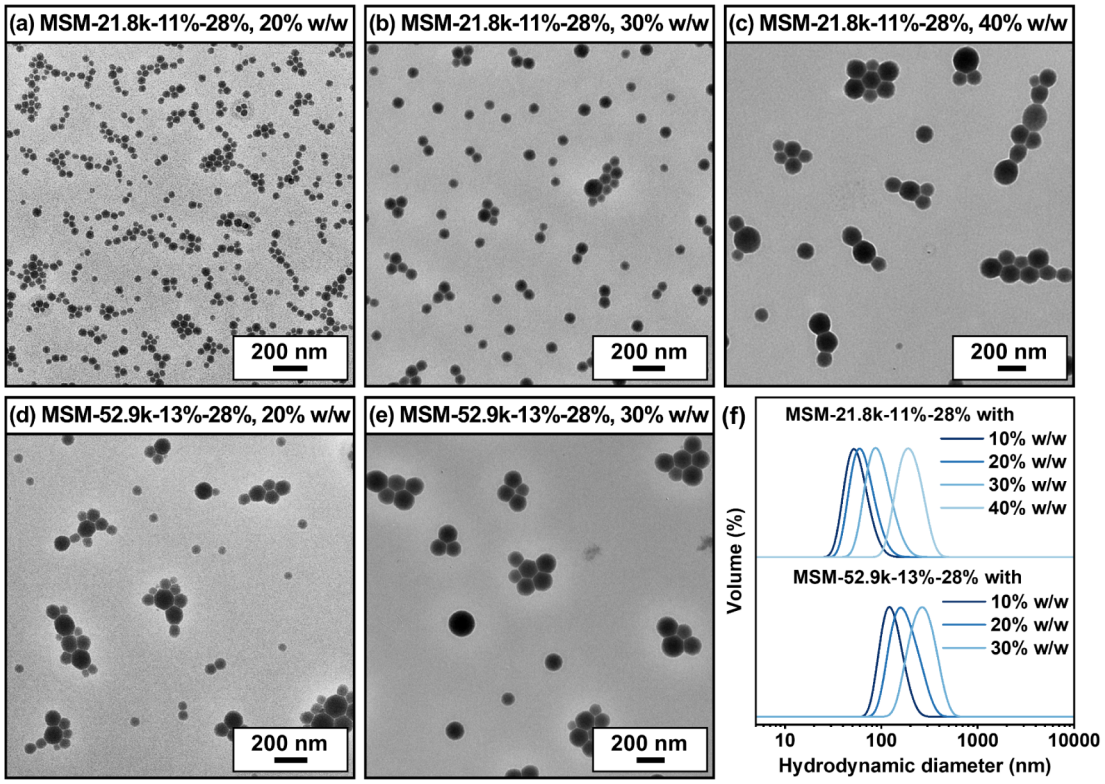

Figure 4. TEM images of nano-objects (diluted as 0.05−0.1% w/w dispersion in toluene) generated by HISA process in DMF with different solids content from (**a**−**c**) MSM-21.8k-11%-28%, (**d**, **e**) MSM-52.9k-13%-28% triblock copolymers. (**f**) DLS results of the corresponding nano-objects in toluene.

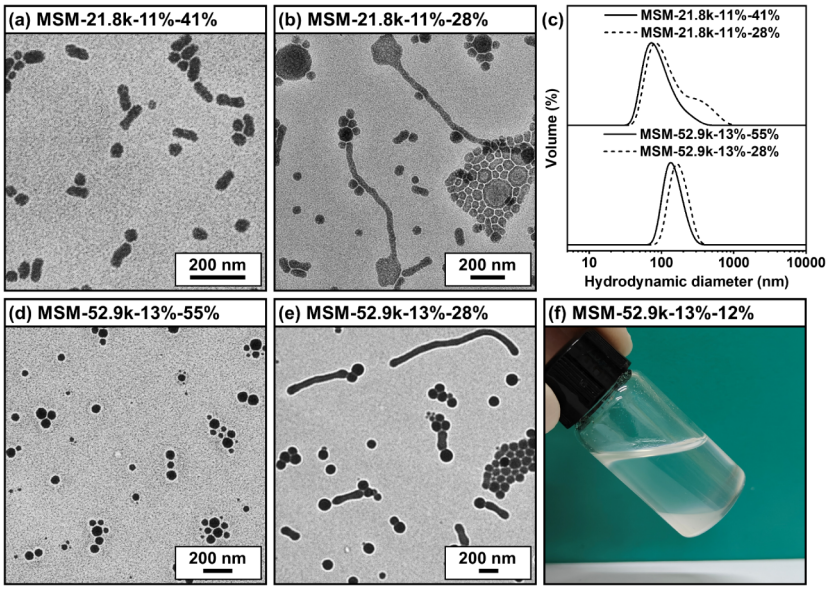

Figure 5. TEM images of nano-objects (diluted as 0.03−0.06% w/w dispersion in THF) generated by HISA process in ethanol/water (8/2 v/v) mixture with solids content of 2% w/w from (**a**) MSM-21.8k-11%-41%, (**b**) MSM-21.8k-11%-28%, (**d**) MSM-52.9k-13%-55%, (**e**) MSM-52.9k-13%-28%, and (**f**) MSM-52.9k-13%-12% triblock copolymers. (**c**) DLS results of the corresponding nano-objects in THF.

with lower PMMA content exhibited slightly larger sizes, which were consistently verified by the DLS results (Figure 2c,f,i). Specifically, for copolymers with a fixed core-forming block length, more block copolymers tended to aggregate and form larger nano-objects when the stabilizer block length decreased, which obeyed the general self-assembly principles for BCPs.[43−46]

Subsequently, fixing the core-forming block as P(DMS-*co*-VMS)-52.9k-13% with a relatively higher MW, the nano-objects of different sizes were prepared from MSM-52.9k-13%-z triblock copolymers with different MWs of the PMMA block (Figure 3). Similarly, all the samples formed nano-objects with a spherical morphology. Differently, as the PMMA content decreased, the sizes of the nano-objects formed from MSM-

https://doi.org/10.1021/acsapm.5c04232
ACS Appl. Polym. Mater. 2026, 8, 2731−2745

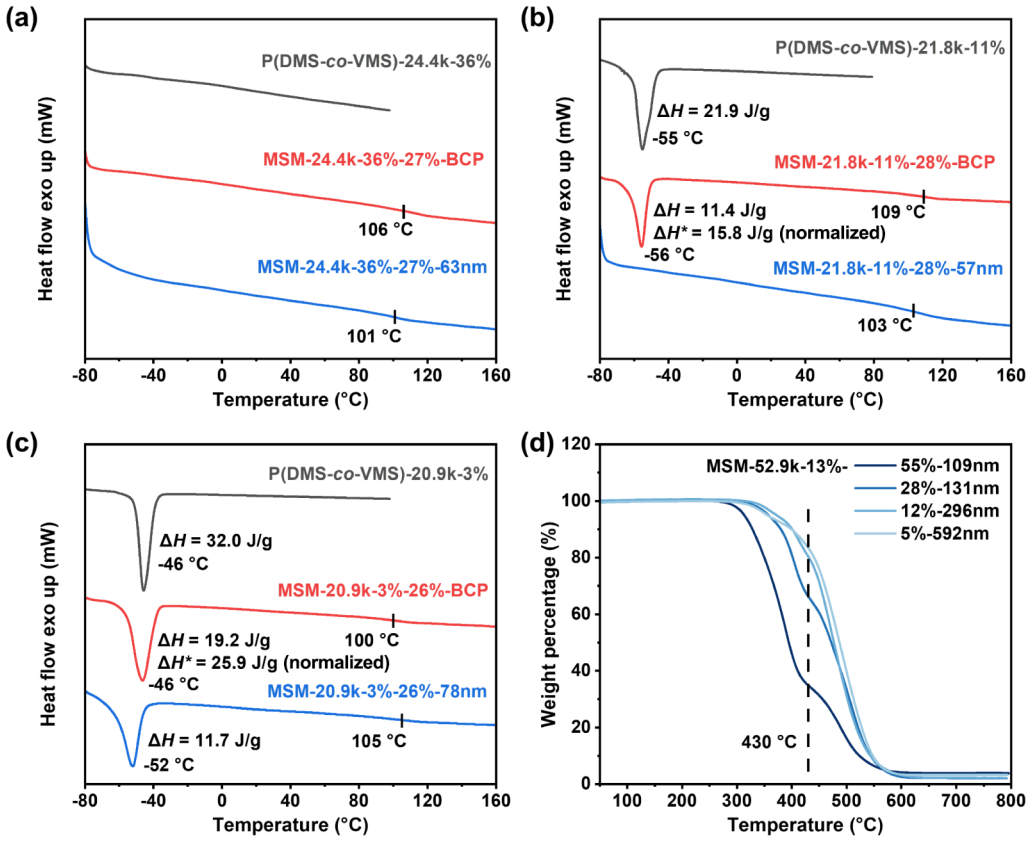

Figure 6. DSC curves for (**a**) MSM-24.4k-36%-27%, (**b**) MSM-21.8k-11%-28%, and (**c**) MSM-20.9k-3%-26% nano-objects and the corresponding triblock copolymers and P(DMS-*co*-VMS) precursor. (**d**) TGA curves for MSM-52.9k-13%-z-s nano-objects.

52.9k-13%-55%, MSM-52.9k-13%-28%, MSM-52.9k-13%-12%, and MSM-52.9k-13%-5% increased regularly. The TEM images and DLS curves revealed consistent results. Notably, the nano-objects formed from MSM-52.9k-13%-12% increased to 296 nm, and those from MSM-52.9k-13%-5% further increased to 592 nm. In both cases, the spheres were severely aggregated, which could be attributed to the relatively shorter stabilizer length of the PMMA block, resulting in fusion between different nano-objects.

Meanwhile, taking MSM-21.8k-11%-28% and MSM-52.9k-13%-28% as examples, the effect of the solids content on the HISA process was further investigated (Figure 4). For MSM-21.8k-11%-28%, as the solids content during the HISA process was increased from 10% to 20%, 30%, and 40% w/w, the sizes of the nano-objects regularly increased from 57 to 66, 97, and 203 nm, while maintaining their spherical morphology. Similarly, for MSM-52.9k-13%-28%, when the solids content was increased from 10% to 20% w/w, the sizes of the spherical nano-objects also increased from 131 to 181 nm, and further increased to 275 nm when the solids content reached 30% w/w. Clearly, the sizes of the nano-objects increased with the rising solids content. This could be attributed to the fact that, at higher solids content, more triblock copolymers tended to aggregate and incorporated into a single nano-object, thereby leading to an increase in the sizes of the nano-objects.

According to the literature,[47,48] a specific ratio of ethanol/water (8/2 v/v) mixture served as a unique solvent for PMMA, offering better biocompatibility and low toxicity. Thus, the ethanol/water (8/2 v/v) mixture was also employed as a selective solvent for the HISA process of the MSM triblock copolymer with a solids content of 2% w/w. As shown in Figure 5a, after diluting and dispersing the nano-objects into THF, the nano-objects with spherical and short worm-like morphologies were obtained from MSM-21.8k-11%-41%. For MSM-21.8k-11%-28%, which had relatively lower PMMA content, longer worms and "tadpole-like" nano-objects were further observed (Figure 5b). Alternatively, the nano-objects with spherical morphology were obtained from MSM-52.9k-13%-55% (Figure 5d). When the PMMA content was reduced to 28%, a worm-like morphology was also observed for MSM-52.9k-13%-28% (Figure 5e). Further reduction of the PMMA content to 12% resulted in precipitation for MSM-52.9k-13%-12% (Figure 5f). Compared to the HISA process in DMF, the MSM triblock copolymers tended to form higher-order morphologies in the ethanol/water (8/2 v/v) mixture. This might be due to the relatively poor solubility of PMMA chains in the ethanol/water (8/2 v/v) mixture compared to the DMF solvent. For a similar reason, the relatively low solids content of 2% w/w was successful for the HISA process, while higher solids content resulted in the formation of precipitates. Herein, the HISA process in the DMF and ethanol/water (8/2 v/v) mixture was the same, and thus the effect of temperature could be excluded. Alternatively, the solubility of PMMA and P(DMS-*co*-VMS), i.e., solubility parameter, should dominantly affect the self-assembly behavior. In fact, the distinct solubility of MSM triblock copolymer can be quantified and discriminated by the solubility parameters of DMF (24.1 $MPa^{1/2}$), ethanol (26.0 $MPa^{1/2}$), water (47.9 $MPa^{1/2}$), PMMA (19.0 $MPa^{1/2}$), and PDMS (14.9 $MPa^{1/2}$).[49−51] Due to the structural similarity, the P(DMS-*co*-VMS) can be regarded as the analogue of PDMS and has a similar solubility parameter. Obviously, the solubility parameter of DMF is much closer to

https://doi.org/10.1021/acsapm.5c04232
ACS Appl. Polym. Mater. 2026, 8, 2731−2745

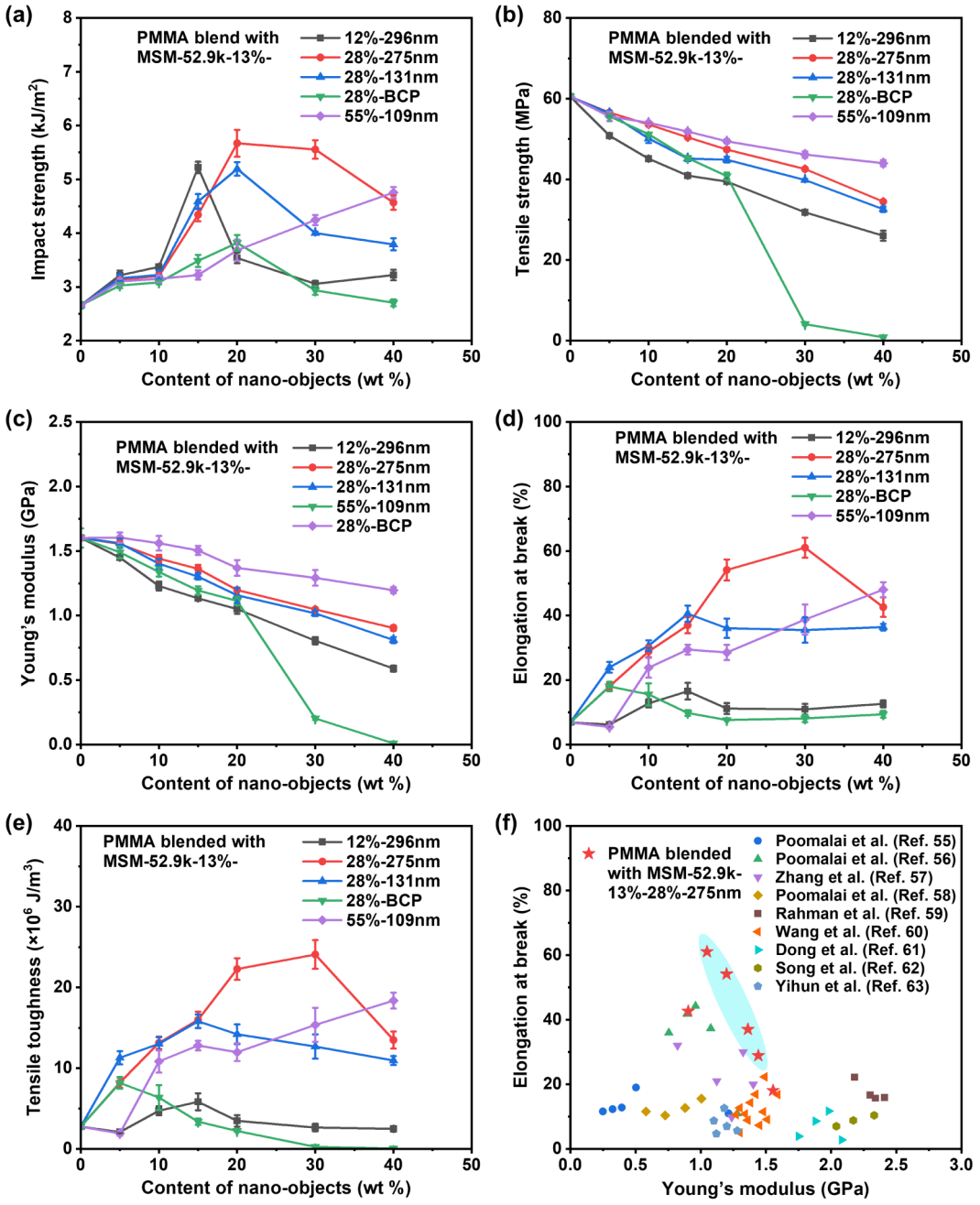

Figure 7. (a) Impact strength, (b) tensile strength, (c) Young's modulus, (d) elongation at break, (e) tensile toughness versus the content of nano-objects. (f) Ashby plot showing the elongation at break versus Young's modulus of toughened PMMA.[55−63]

those of PMMA and PDMS or P(DMS-*co*-VMS). The solubility parameter of ethanol/water (8/2 v/v) mixture can be calculated as 30.4 $MPa^{1/2}$ based on the solubility parameters of ethanol and water, which is actually higher than those of PMMA and PDMS or P(DMS-*co*-VMS). Additionally, the PMMA homopolymer had been confirmed with an upper critical solution temperature (UCST) around 34 °C in ethanol/water (8/2 v/v) mixture,[48] while no such temperature could be detected in DMF. Correspondingly, following the general self-assembly principle, the higher-order morphologies were favored by the poor solvents, such as ethanol/water (8/2 v/v) mixture, which tended to reduce the repulsive interactions between the shell-forming block and promoted the aggregation of more block copolymers, leading to the formation of nano-objects with larger sizes and higher-order morphologies.

3.3. Thermal Properties of Polysiloxane-Based Nano-Objects

As mentioned in Section 1, polysiloxane exhibits excellent resistance to extremely high or low temperatures. Herein, the nano-objects prepared above are expected to have a soft P(DMS-*co*-VMS) core and a hard PMMA shell. Correspondingly, the thermal properties of the polysiloxane-based nano-objects were comprehensively evaluated by differential scanning calorimetry (DSC) and thermogravimetric analysis (TGA) measurements, confirming the anticipated structure and soft-core characteristics. For comparison, in the following section, the MSM-x-y-z triblock copolymers are labeled as

https://doi.org/10.1021/acsapm.5c04232
ACS Appl. Polym. Mater. 2026, 8, 2731−2745

MSM-x-y-z-BCP, and the self-assembled nano-objects are labeled as MSM-x-y-z-s, where "s" represents the size of the MSM nano-objects. From Figure 6a−c, the DSC curves indicated that both the MSM triblock copolymers and the nano-objects exhibited a T_g of PMMA around 105 °C. Differently, no T_m could be detected for the P(DMS-*co*-VMS)-24.4k-36% random copolymer, MSM-24.4k-36%-27% triblock copolymer, and MSM-24.4k-36%-27% nano-objects. This absence of T_m might be due to the lower chain regularity and crystallization of the polysiloxane formed with a high VMS content. Alternatively, the T_m at −55 and −56 °C were clearly observed for the P(DMS-*co*-VMS)-21.8k-11% random copolymer and MSM-21.8k-11%-28% triblock copolymer, respectively. In this case, the VMS content was lowered, and the crystallization behavior of the polysiloxane could be observed. Compared to the melting enthalpy of P(DMS-*co*-VMS)-21.8k-11% (21.9 J/g), the melting enthalpy of P(DMS-*co*-VMS) in the MSM triblock copolymer was relatively low (15.8 J/g, normalized by the mass fraction of P(DMS-*co*-VMS)). The reason might be attributed to the PMMA blocks at both ends, which greatly hindered the movement and crystallization of the middle P(DMS-*co*-VMS) block. However, the T_m for the MSM-21.8k-11%-28% nano-objects disappeared. The reason could be attributed to the disruption of the crystallization of the P(DMS-*co*-VMS) core during the cross-linking process. Furthermore, for the P(DMS-*co*-VMS)-20.9k-3% random copolymer, MSM-20.9k-3%-26% triblock copolymer, and their corresponding nano-objects, the T_m could be clearly observed in all three DSC curves at −46 °C, −46 °C, and −52 °C, respectively. In this case, the VMS content was significantly decreased, and the crystallization of the random copolymers was thus enhanced. Similarly, the melting enthalpies for the P(DMS-*co*-VMS)-20.9k-3% precursor, MSM-20.9k-3%-26% triblock copolymer, and MSM-20.9k-3%-26% nano-objects were also regularly decreased from 32.0 J/g to 19.2 J/g and 11.7 J/g, respectively. The presence of T_m in the DSC curves convincingly confirmed that the nano-objects had a lower cross-linking density, which did not significantly disrupt the crystallization behavior of the P(DMS-*co*-VMS) core. As expected, for all samples, the low T_m around −50 °C confirmed that the nano-objects actually have a soft-core character. Additionally, it should be mentioned that both the T_g of PDMS (around −120 °C) and PVMS (around −100 °C) are below the detection range of the instrument and therefore cannot be observed in DSC curves.[40−42]

Meanwhile, the TGA results were listed in Figure 6d. The TGA curves indicated that the PMMA shell on the nano-objects started to decompose at about 300 °C, reaching the maximum weight loss rate around 400 °C. The P(DMS-*co*-VMS) core exhibited improved thermal stability, decomposing after the PMMA and reaching the maximum weight loss rate at about 500 °C. At the inflection point around 430 °C, the weight loss percentage was slightly higher than the mass fraction of PMMA shown in Table 1, which might be attributed to the decomposition of side groups in the P(DMS-*co*-VMS) before that of the O−Si−O main chain.[52]

3.4. Toughening Behavior of PMMA Mixed with Polysiloxane-Based Nano-Objects

As confirmed by the thermal characterizations above, the P(DMS-*co*-VMS) core has a lower T_g and T_m, which endows the nano-objects with the potential to function as toughening agents. Meanwhile, the PMMA shell exhibits excellent miscibility with the PMMA matrix, facilitating the dispersion of the nano-objects and maximizing the improvement of the composite properties. For comparison, the MSM-52.9k-13%-12%-296 nm, MSM-52.9k-13%-28%-275 nm, MSM-52.9k-13%-28%-131 nm, and MSM-52.9k-13%-55%-109 nm nano-objects, which have different sizes and chain lengths of PMMA, were selectively employed as toughening agents for the PMMA matrix. Additionally, the MSM-52.9k-13%-28%-BCP triblock copolymer was chosen as a control for comparison.

Typically, for toughening applications, smaller particles are more effective in inducing shear deformation and crazing, while larger particles can absorb more energy to inhibit the propagation of crazes, with the optimal particle size being around 250 nm.[53,54] From the impact strength results (Figure 7a), it could be discriminated that the composite containing the MSM-52.9k-13%-12%-296 nm, MSM-52.9k-13%-28%-275 nm, and MSM-52.9k-13%-28%-131 nm nano-objects exhibited maximum impact strength at mass fractions of either 15 or 20 wt %. For instance, at a nano-object mass fraction of 20 wt %, the composite containing MSM-52.9k-13%-28%-275 nm nano-objects has an impact strength of 5.67 kJ/m^2, representing a 113% increase compared to pure PMMA's 2.66 kJ/m^2. Differently, the impact strength of the composite containing the MSM-52.9k-13%-55%-109 nm nano-object consistently increased with the increase in the mass fraction of nano-objects in the range of 0−40 wt %. By analyzing the differences among these four nano-objects, several key reasons could be proposed. First, the mass fraction of nano-objects affected the impact strength. A higher mass fraction of nano-objects introduced a greater content of P(DMS-*co*-VMS), which could correspondingly improve the impact strength. Second, the content and chain length of the PMMA shell on the nano-objects also influenced impact strength. When the PMMA in the shell layer was relatively short, there was insufficient entanglement with the PMMA matrix, which affected the energy transfer within the material. However, an increase in the content and chain length of PMMA also implied a decrease in the content of P(DMS-*co*-VMS), which adversely affected the impact strength. Third, as mentioned earlier, the size of the nano-objects affected toughening performance, which was primarily modulated by the MW of the MSM triblock copolymers and the solids content during the HISA process. Thus, the mass fraction of nano-objects, the content and chain length of the PMMA shell, and the sizes of the nano-objects synergistically affected impact strength. It could be noticed that the smaller size of the MSM-52.9k-13%-55%-109 nm nano-objects had a longer PMMA shell and lower P(DMS-*co*-VMS) content, which thus required a higher content to improve impact strength. Alternatively, the larger sizes of the MSM-52.9k-13%-12%-296 nm and MSM-52.9k-13%-28%-275 nm nano-objects exhibited maximum impact strength at lower content levels. Compared to the MSM-52.9k-13%-28%-275 nm and MSM-52.9k-13%-28%-131 nm nano-objects with the same compositions, the composite containing MSM-52.9k-13%-28%-BCP as a toughening agent exhibited the lowest impact strength, which might be attributed to the worse dispersion of the MSM triblock copolymer compared to the regular nano-objects, resulting in an inferior toughening function. That was, the formation of regular morphologies and controlled sizes should be the intrinsic reason for the performance improvement of the composite.

Meanwhile, the tensile properties of the composites mentioned above were also investigated (Figure S4, Figure

https://doi.org/10.1021/acsapm.5c04232
ACS Appl. Polym. Mater. 2026, 8, 2731−2745

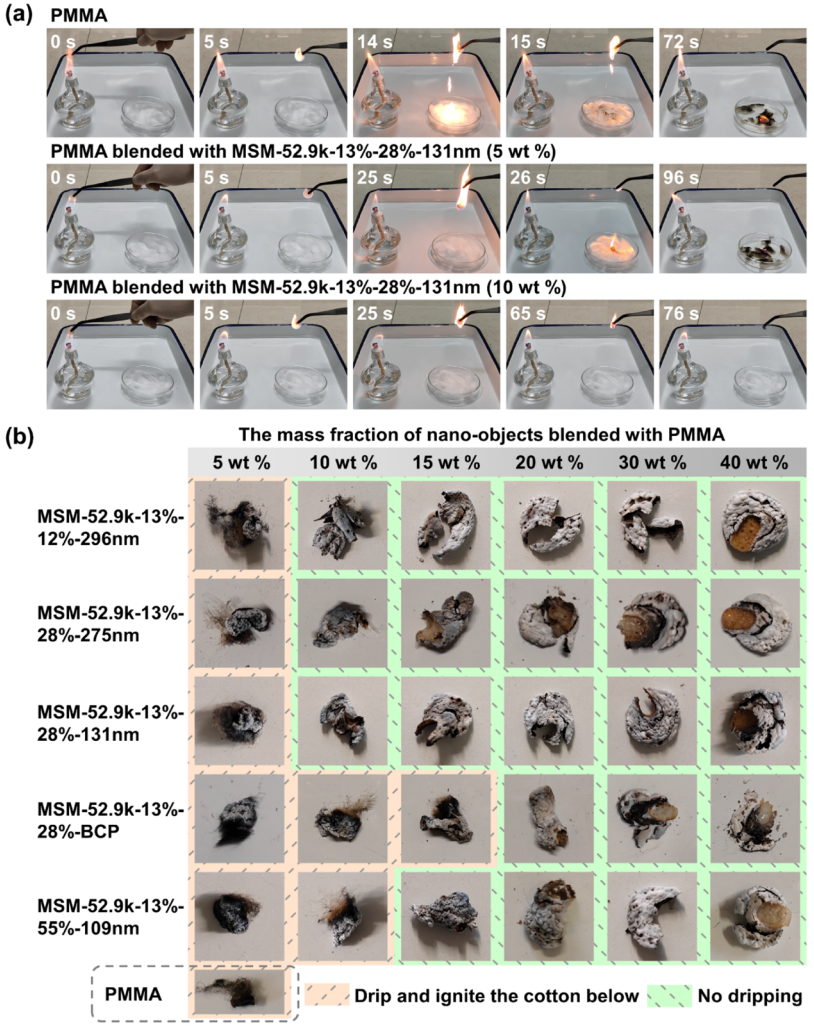

Figure 8. (a) Combustion process at different times of PMMA, PMMA blended with MSM-52.9k-13%-28%-131 nm (5 wt %), and PMMA blended with MSM-52.9k-13%-28%-131 nm (10 wt %). (b) Photos of the residue after combustion. For the samples that dripped, the residues adhered to the cotton.

7b–e). As shown in Figure 7b, the tensile strength regularly decreased with the increase in the mass fraction of nano-objects. Comparatively, the composite containing MSM-52.9k-13%-12%-296 nm nano-objects was more sensitive than those containing MSM-52.9k-13%-28%-275 nm, MSM-52.9k-13%-28%-131 nm, and MSM-52.9k-13%-55%-109 nm nano-objects. Also, the Young's modulus showed a similar trend. From Figure 7d,e, it could be noticed that the elongation at break and tensile toughness of the composite containing MSM-52.9k-13%-28%-275 nm, MSM-52.9k-13%-28%-131 nm, and MSM-52.9k-13%-55%-109 nm nano-objects were superior to those of the composite containing MSM-52.9k-13%-12%-296 nm nano-objects. Again, the reason might be attributed to the relatively shorter PMMA shell on the MSM-52.9k-13%-12%-296 nm nano-objects, which has less entanglement with the PMMA matrix, further confirming the dominant effect of the PMMA shell on the mechanical properties of the composite. Due to the favorable balance between the content and chain length of PMMA, as well as the appropriate size of the nano-objects, the PMMA modified with MSM-52.9k-13%-28%-275 nm exhibited excellent elongation at break and tensile toughness at mass fractions of 20 and 30 wt %. Notably, at a mass fraction of 30 wt %, the elongation at break reached 61%, and the tensile toughness reached 24.08 × 10^6 J/m^3, representing a 774% increase compared to the 2.75 × 10^6 J/m^3 of pure PMMA. Comparatively, for MSM-52.9k-13%-28%-BCP, a certain level of toughening performance was observed at a mass fraction of 5 wt %, which might be attributed to the formation of some spherical P(DMS-*co*-VMS) phases through the self-assembly of MSM triblock copolymers within the PMMA matrix. However, as the mass fraction continued to increase, the toughening effect deteriorated due to inferior dispersion and undefined microphases. Particularly, at mass fractions of 30 and 40 wt %, the mechanical properties of the composite were significantly lowered. Generally, the composites exhibited a similar improvement trend in tensile properties to that observed in impact strength.

Additionally, as shown in the Ashby plot (Figure 7f), the modification of PMMA with soft polysiloxane core nano-objects (MSM-52.9k-13%-28%-275 nm) resulted in a high elongation at break while maintaining a relatively considerable Young's modulus, due to the excellent flexibility of polysiloxane. That was, the comprehensive mechanical properties of the composite could be enhanced by introducing the soft polysiloxane core nano-objects.

https://doi.org/10.1021/acsapm.5c04232
ACS Appl. Polym. Mater. 2026, 8, 2731–2745

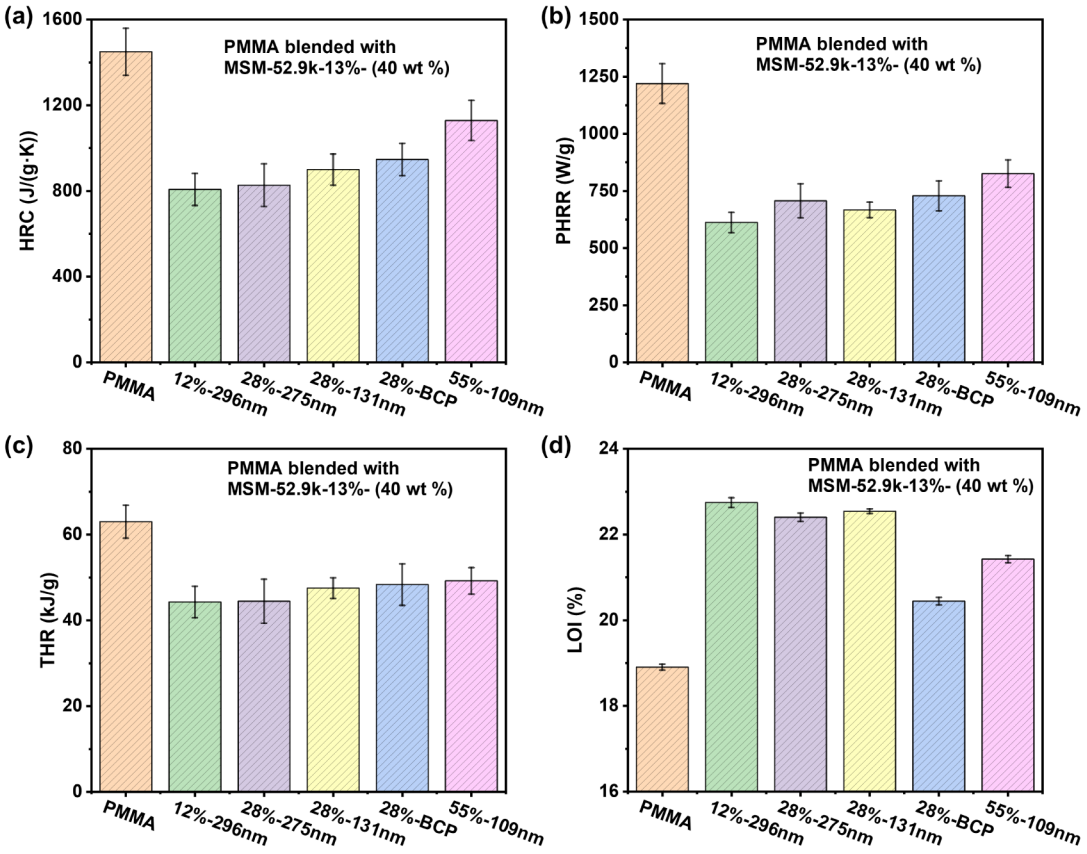

Figure 9. (a) HRC, (b) PHRR, and (c) THR of PMMA matrix and composites based on MCC measurements. (d) LOI of PMMA matrix and composites.

3.5. Flame-Retardant Performance of PMMA Mixed with Polysiloxane-Based Nano-Objects

During a combustion process, the function of flame-retardant performance is especially important.[64,65] Generally, silicon is a widely used element in flame-retardant materials. During combustion, silicon can form a cross-linked network that prevents thermoplastic polymers from dripping and promotes the formation of a dense char layer.[7,8,66,67] Thus, in addition to the above toughening modification, the combustion process of the composite was also investigated. As the photos shown in Figure 8a, during the combustion of PMMA, several instances of dripping occurred, and the dripped material instantly ignited the cotton below. When the PMMA matrix was blended with 5 wt % MSM-52.9k-13%-28%-131 nm nano-objects, dripping during combustion was suppressed, and only one drop was observed, which similarly ignited the underlying cotton. When the content of MSM-52.9k-13%-28%-131 nm nano-objects was increased to 10 wt %, no dripping occurred during the whole combustion process. Clearly, the higher content of nano-objects effectively prevented dripping.

Furthermore, the photos of the postcombustion residue of PMMA blended with different mass fractions (5, 10, 15, 20, 30, and 40 wt %) of MSM-52.9k-13%-12%-296 nm, MSM-52.9k-13%-28%-275 nm, MSM-52.9k-13%-28%-131 nm, MSM-52.9k-13%-28%-BCP, and MSM-52.9k-13%-55%-109 nm are summarized in Figure 8b. In comparison, the PMMA matrix favored dripping and left only a small amount of black burnt residue after combustion. When the mass fractions of MSM-52.9k-13%-12%-296 nm, MSM-52.9k-13%-28%-275 nm, and MSM-52.9k-13%-28%-131 nm exceeded 10 wt %, no dripping was observed. For MSM-52.9k-13%-55%-109 nm, dripping ceased at mass fractions above 15 wt % due to the relatively lower content of P(DMS-*co*-VMS) in the nano-objects. Clearly, for all samples, a higher content of nano-objects and P(DMS-*co*-VMS) increased the likelihood of forming a denser char layer on the surface of the combusted material. By normalizing the P(DMS-*co*-VMS) content in all nano-object-based composites (Table S1), it could be evaluated that approximately 7 wt % P(DMS-*co*-VMS) was sufficient to prevent the combustion dripping of the PMMA matrix. However, for MSM-52.9k-13%-28%-BCP, which has the same composition as MSM-52.9k-13%-28%-275 nm and MSM-52.9k-13%-28%-131 nm nano-objects, a higher mass fraction of 20 wt % MSM and approximately 14 wt % P(DMS-*co*-VMS) was required to prevent dripping. Similarly, the reason might be due to the inferior dispersion of the MSM triblock copolymers in the PMMA matrix. Again, these results confirmed that the formation of regular morphologies was essential for the enhanced flame-retardant properties. That was, the self-assembly is actually an efficient method to introduce functional polysiloxane into the composite.

To further evaluate the flame-retardant performance, the composites with 40 wt % nano-object content were selected for microscale combustion calorimetry (MCC) and limiting oxygen index (LOI) testing. From Figure S5, compared to the pure PMMA matrix, the MCC curves of the composites exhibited a significant decrease, indicating that their heat release was suppressed. Additionally, a small peak appeared around 520 °C, which represented the heat release of the polysiloxane. The heat release capacity (HRC), peak heat

https://doi.org/10.1021/acsapm.5c04232
ACS Appl. Polym. Mater. 2026, 8, 2731−2745

release rate (PHRR), and total heat release (THR) are summarized in Figure 9a−c and Table S2. Corresponding to the MCC curves, all of these parameters for the composites were reduced and showed a decreasing trend with the increase in polysiloxane content. Also, the LOI results further demonstrated the improved flame-retardant performance (Figure 9d, Table S2). Similarly, a higher polysiloxane content provided enhanced flame-retardant properties. The LOI of the PMMA blended with MSM-52.9k-13%-12%-296 nm (40 wt %) composite increased from 18.9% for pure PMMA to 22.7%. The improved flame-retardant performance can be attributed to the polysiloxane promoting char formation, which isolated oxygen and weakened heat and mass transfer during combustion. Notably, the composite of PMMA blended with MSM-52.9k-13%-28%-BCP (40 wt %) showed a lower LOI (20.4%), which might be due to the inferior dispersion of MSM triblock copolymers, rather than the nano-objects with regular morphologies. Actually, this result emphasized that the formation of nano-objects was essential for an improved flame-retardant performance.

4. CONCLUSIONS

In summary, by means of the powerful HISA process, we successfully prepared a series of polysiloxane-based soft-core nano-objects from MSM triblock copolymers. First, the MSM triblock copolymer was designed and synthesized from a difunctional initiator, DBDAM, which is a bifunctional initiator for both ROP and ATRP mechanisms. Subsequently, employing DMF or an ethanol/water (8/2 v/v) mixture as selective solvents, the nano-objects with spherical and worm-like morphologies were fabricated and monitored by TEM measurement. Using the vinyl group in P(DMS-*co*-VMS) core, the nano-objects could be *in situ* stabilized by an EDT agent and well-dispersed in good solvents of toluene or THF. Effectively, the DSC results confirmed the formation of a soft core in the nano-objects. Furthermore, the nano-objects with regular morphologies, controlled sizes, adjustable cross-linking densities, tunable PMMA contents, and block lengths have significant improvement on the toughening and flame-retardant performance of PMMA-based composites, obviously superior to the counterpart of MSM triblock copolymer with undefined microphase. Under optimized conditions, such as with MSM-52.9k-13%-28%-275 nm, it demonstrates that HISA is a powerful strategy for introducing soft functional polysiloxane into advanced materials and practical applications. However, in the present work, the synthesis of MSM triblock copolymers and functional toughening behavior or flame-retardant performance were just a proof of concept. Further practical applications still require the synthesis of well-defined MSM triblock copolymers on a large scale and in an efficient route, improved performance of nano-objects with optimal factors, and the investigation of long-term thermal-oxidative aging or damp-heat cycling performance. In the future, further addressing these questions would facilitate more practical applications of the explored soft polysiloxane core nano-objects.

■ ASSOCIATED CONTENT

Supporting Information

The Supporting Information is available free of charge at https://pubs.acs.org/doi/10.1021/acsapm.5c04232.

Testing and characterization methods; ^{1}H NMR and ^{13}C NMR spectra of DAM and DBDAM (Figure S1); additional SEC traces for P(DMS-*co*-VMS) and the corresponding MSM triblock copolymers (Figure S2); ^{29}Si NMR spectrum for P(DMS-*co*-VMS)-24.4k-36% (Figure S3); the stress−strain curves of toughened PMMA composite (Figure S4); the data for PMMA-based composites (Table S1); MCC curves for PMMA matrix and PMMA composite (Figure S5); the HRC, PHRR, THR, and LOI of PMMA matrix and composites (Table S2) (PDF)

■ AUTHOR INFORMATION

Corresponding Authors

Guowei Wang − *State Key Laboratory of Molecular Engineering of Polymers, Department of Macromolecular Science, Fudan University, Shanghai 200438, China;* orcid.org/0000-0003-2595-8269; Email: gwwang@fudan.edu.cn

Xiangcheng Pan − *State Key Laboratory of Molecular Engineering of Polymers, Department of Macromolecular Science, Fudan University, Shanghai 200438, China;* orcid.org/0000-0003-3344-4639; Email: panxc@fudan.edu.cn

Authors

Yu Hu − *State Key Laboratory of Molecular Engineering of Polymers, Department of Macromolecular Science, Fudan University, Shanghai 200438, China*

Jingwei Zhang − *State Key Laboratory of Molecular Engineering of Polymers, Department of Macromolecular Science, Fudan University, Shanghai 200438, China*

Hanyu Lv − *State Key Laboratory of Molecular Engineering of Polymers, Department of Macromolecular Science, Fudan University, Shanghai 200438, China*

Boyang Shi − *State Key Laboratory of Molecular Engineering of Polymers, Department of Macromolecular Science, Fudan University, Shanghai 200438, China*

Jiali Wu − *State Key Laboratory of Molecular Engineering of Polymers, Department of Macromolecular Science, Fudan University, Shanghai 200438, China*

Complete contact information is available at: https://pubs.acs.org/10.1021/acsapm.5c04232

Author Contributions

Y.H.: conceptualization, data curation, formal analysis, investigation, methodology, visualization, writing—original draft. J.Z.: data curation, formal analysis, software, writing—original draft. H.L.: data curation, formal analysis. B.S.: formal analysis. J.W.: formal analysis. X.P.: conceptualization, supervision, writing-review and editing. G.W.: conceptualization, funding acquisition, project administration, resources, supervision, writing—review and editing.

Notes

The authors declare no competing financial interest.

■ ACKNOWLEDGMENTS

This work is supported by the National Natural Science Foundation of China (21574022, 22322103, and 22271057).

REFERENCES

(1) Yang, X.; Huang, W.; Dong, H.; Zha, J.-W. Smart Polydimethylsiloxane Materials: Versatility for Electrical and Electronic Devices Applications. *Adv. Mater.* **2025**, *37* (17), 2500472.

(2) Wang, H.; Chen, S.; Li, Y.; Liu, Y.; Jing, Q.; Liu, X.; Liu, Z.; Zhang, X. Organosilicon-Based Functional Electrolytes for High-performance Lithium Batteries. *Adv. Energy Mater.* **2021**, *11* (28), 2101057.

(3) Zhao, X. Z.; Liang, Y.; Wang, T.; Li, F. F.; Wang, H. Self-Assembled Porous Nanoparticles Based on Silicone Polymers with Aggregation-Induced Emission for Highly Sensitive Detection of Nitroaromatics. *Polym. Chem.* **2021**, *12* (48), 7016−7022.

(4) Zhang, X.; Ge, A.; Tang, Y.; Wei, W.; Li, X. Facile Synthesis of P-Functionalized Diphenyl-Methylvinyl-Copolysiloxane for High-Performance Epoxy Thermosets. *Eur. Polym. J.* **2025**, *231*, 113903.

(5) Romo-Uribe, A.; Santiago-Santiago, K.; Reyes-Mayer, A.; Aguilar-Franco, M. Functional PDMS Enhanced Strain at Fracture and Toughness of DGEBA Epoxy Resin. *Eur. Polym. J.* **2017**, *89*, 101−118.

(6) Demleitner, M.; Schönl, F.; Angermann, J.; Fässler, P.; Lamparth, I.; Rist, K.; Schnur, T.; Catel, Y.; Rosenfeldt, S.; Retsch, M.; et al. Influence of Block Copolymer Concentration and Resin Crosslink Density on the Properties of UV-curable Methacrylate Resin Systems. *Macromol. Mater. Eng.* **2022**, *307* (10), 2200320.

(7) Fan, S.; Peng, B.; Yuan, R.; Wu, D.; Wang, X.; Yu, J.; Li, F. A Novel Schiff Base-Containing Branched Polysiloxane as a Self-Crosslinking Flame Retardant for PA6 with Low Heat Release and Excellent Anti-Dripping Performance. *Composites, Part B* **2020**, *183*, 107684.

(8) Yang, S.; Lv, G.; Liu, Y.; Wang, Q. Synergism of Polysiloxane and Zinc Borate Flame Retardant Polycarbonate. *Polym. Degrad. Stab.* **2013**, *98* (12), 2795−2800.

(9) Zhang, T.; Hu, Q.; Yu, J.; Han, X.; Jiao, J.; Yuan, H.; Zhang, R.; Qi, J.; Gao, D.; Glebe, U.; et al. A Facile and Efficient Route to Achieve Polythiophene-Based Nanoparticles with Various Morphologies. *Angew. Chem., Int. Ed.* **2025**, *64* (43), No. e202502460.

(10) Penfold, N. J. W.; Yeow, J.; Boyer, C.; Armes, S. P. Emerging Trends in Polymerization-Induced Self-Assembly. *ACS Macro Lett.* **2019**, *8* (8), 1029−1054.

(11) Li, C.; Li, Q.; Kaneti, Y. V.; Hou, D.; Yamauchi, Y.; Mai, Y. Self-Assembly of Block Copolymers towards Mesoporous Materials for Energy Storage and Conversion Systems. *Chem. Soc. Rev.* **2020**, *49* (14), 4681−4736.

(12) Ji, H. X.; Wang, W. Z.; Li, X.; Han, X. Y.; Zhang, X. Y.; Wang, J.; Liu, C. X.; Huang, L. Q.; Gao, W. Y. Natural Small Molecules Enabled Efficient Immunotherapy through Supramolecular Self-Assembly in P53-Mutated Colorectal Cancer. *ACS Appl. Mater. Interfaces* **2022**, *14* (2), 2464−2477.

(13) Shi, B.; Shen, D.; Li, W.; Wang, G. Self-Assembly of Copolymers Containing Crystallizable Blocks: Strategies and Applications. *Macromol. Rapid Commun.* **2022**, *43* (14), 2200071.

(14) Liu, Q.-J.; Liu, Q.; Zhang, J.; Zhang, C.; Qian, L.; Qi, H.; Li, Y.-S.; Song, D.-P. Photonic Microspheres for High-Capacity DNA Data Storage: Robust, Straightforward, and Scalable Random Access via Nonfading Indexes. *Sci. Adv.* **2025**, *11* (25), No. eadw2613.

(15) Guo, Q.; Xue, R.; Zhao, J.; Zhang, Y.; Van De Kerkhof, G. T.; Zhang, K.; Li, Y.; Vignolini, S.; Song, D.-P. Precise Tailoring of Polyester Bottlebrush Amphiphiles toward Eco-Friendly Photonic Pigments via Interfacial Self-Assembly. *Angew. Chem., Int. Ed.* **2022**, *61* (34), No. e202206723.

(16) Guo, Q.; Li, Y.; Liu, Q.; Li, Y.; Song, D.-P. Janus Photonic Microspheres with Bridged Lamellar Structures via Droplet-Confined Block Copolymer Co-Assembly. *Angew. Chem., Int. Ed.* **2022**, *61* (5), No. e202113759.

(17) Jennings, J.; Cornel, E. J.; Derry, M. J.; Beattie, D. L.; Rymaruk, M. J.; Deane, O. J.; Ryan, A. J.; Armes, S. P. Synthesis of High χ−Low N Diblock Copolymers by Polymerization-Induced Self-Assembly. *Angew. Chem., Int. Ed.* **2020**, *59* (27), 10848−10853.

(18) Rymaruk, M. J.; O'Brien, C. T.; Brown, S. L.; Williams, C. N.; Armes, S. P. Effect of Core Cross-Linking on the Physical Properties of Poly(dimethylsiloxane)-Based Diblock Copolymer Worms Prepared in Silicone Oil. *Macromolecules* **2019**, *52* (18), 6849−6860.

(19) Rymaruk, M. J.; Hunter, S. J.; O'Brien, C. T.; Brown, S. L.; Williams, C. N.; Armes, S. P. RAFT Dispersion Polymerization in Silicone Oil. *Macromolecules* **2019**, *52* (7), 2822−2832.

(20) Alzahrani, A.; Zhou, D. W.; Kuchel, R. P.; Zetterlund, P. B.; Aldabbagh, F. Polymerization-Induced Self-Assembly Based on ATRP in Supercritical Carbon Dioxide. *Polym. Chem.* **2019**, *10* (21), 2658−2665.

(21) Lopez-Oliva, A. P.; Warren, N. J.; Rajkumar, A.; Mykhaylyk, O. O.; Derry, M. J.; Doncom, K. E. B.; Rymaruk, M. J.; Armes, S. P. Polydimethylsiloxane-Based Diblock Copolymer Nano-Objects Prepared in Nonpolar Media via RAFT-Mediated Polymerization-Induced Self-Assembly. *Macromolecules* **2015**, *48* (11), 3547−3555.

(22) Nunns, A.; Whittell, G. R.; Winnik, M. A.; Manners, I. Crystallization-Driven Solution Self-Assembly of μ-ABC Miktoarm Star Terpolymers with Core-Forming Polyferrocenylsilane Blocks. *Macromolecules* **2014**, *47* (23), 8420−8428.

(23) Zhang, T.; Jiang, H.; Hong, L.; Ngai, T. Multiple Pickering Emulsions Stabilized by Surface-Segregated Micelles with Adaptive Wettability. *Chem. Sci.* **2022**, *13* (36), 10752−10758.

(24) Tian, J.; Xie, S. H.; Borucu, U.; Lei, S. X.; Zhang, Y. F.; Manners, I. High-Resolution Cryo-Electron Microscopy Structure of Block Copolymer Nanofibres with a Crystalline Core. *Nat. Mater.* **2023**, *22* (6), 786−792.

(25) Raez, J.; Manners, I.; Winnik, M. A. Nanotubes from the Self-Assembly of Asymmetric Crystalline−coil Poly(ferrocenylsilane−siloxane) Block Copolymers. *J. Am. Chem. Soc.* **2002**, *124* (35), 10381−10395.

(26) Martin, L.; Gurnani, P.; Zhang, J.; Hartlieb, M.; Cameron, N. R.; Eissa, A. M.; Perrier, S. Polydimethylsiloxane-Based Giant Glycosylated Polymersomes with Tunable Bacterial Affinity. *Biomacromolecules* **2019**, *20* (3), 1297−1307.

(27) Pavlović, D.; Lou, Q.; Linhardt, J. G.; Künzler, J. F.; Shipp, D. A. Poly(*N*-vinylpyrrolidone)−Polydimethylsiloxane Amphiphilic ABA Triblock Copolymers. *J. Polym. Sci., Part A: Polym. Chem.* **2017**, *55* (20), 3387−3394.

(28) Spulber, M.; Baumann, P.; Saxer, S. S.; Pieles, U.; Meier, W.; Bruns, N. Poly(*N*-vinylpyrrolidone)-Poly(dimethylsiloxane)-Based Polymersome Nanoreactors for Laccase-Catalyzed Biotransformations. *Biomacromolecules* **2014**, *15* (4), 1469−1475.

(29) Car, A.; Baumann, P.; Duskey, J. T.; Chami, M.; Bruns, N.; Meier, W. pH-Responsive PDMS-*b*-PDMAEMA Micelles for Intracellular Anticancer Drug Delivery. *Biomacromolecules* **2014**, *15* (9), 3235−3245.

(30) Zhao, W.; Fonsny, P.; FitzGerald, P.; Warr, G. G.; Perrier, S. Unexpected Behavior of Polydimethylsiloxane/Poly(2-(dimethylamino)ethyl Acrylate) (Charged) Amphiphilic Block Copolymers in Aqueous Solution. *Polym. Chem.* **2013**, *4* (6), 2140.

(31) Langowska, K.; Palivan, C. G.; Meier, W. Polymer Nanoreactors Shown to Produce and Release Antibiotics Locally. *Chem. Commun.* **2013**, *49* (2), 128−130.

(32) Lim, K. T.; Lee, M. Y.; Hwang, H. S.; Heo, H.; Hong, S. S.; Park, J. M. Synthesis and Properties of Well-Defined Poly(dimethylsiloxane)-*b*-Poly(2-hydroxyethyl methacrylate) Copolymers. *Polym. Bull.* **2001**, *47* (2), 135−142.

(33) Zhang, J.; Shi, B.; Wu, X.; Fang, X.; Liang, X.; Peng, Z.; Wang, G. Expanding the Scope of Self-Assembly: Heat-Induced Self-Assembly of Block Copolymers with High Solids. *Macromolecules* **2025**, *58* (10), 4985−5000.

(34) Chojnowski, J.; Cypryk, M.; Kaźmierski, K. Cationic Polymerization of a Model Cyclotrisiloxane with Mixed Siloxane Units Initiated by a Protic Acid. Mechanism of Polymer Chain Formation. *Macromolecules* **2002**, *35* (27), 9904−9912.

(35) Patnode, W.; Wilcock, D. F. Methylpolysiloxanes. *J. Am. Chem. Soc.* **1946**, *68* (3), 358−363.

https://doi.org/10.1021/acsapm.5c04232
ACS Appl. Polym. Mater. 2026, 8, 2731−2745

(36) Teng, C. J.; Weber, W. P.; Cai, G. Anionic and Cationic Ring-Opening Polymerization of 2,2,4,4,6,6-Hexamethyl-8,8-Divinylcyclotetrasiloxane. *Macromolecules* **2003**, *36* (14), 5126−5130.
(37) Ziemelis, M. J.; Saam, J. C. Sequence Distribution in Poly(dimethylsiloxane-*co*-methylvinylsiloxanes). *Macromolecules* **1989**, *22* (5), 2111−2116.
(38) Truong, N. P.; Jones, G. R.; Bradford, K. G. E.; Konkolewicz, D.; Anastasaki, A. A Comparison of RAFT and ATRP Methods for Controlled Radical Polymerization. *Nat. Rev. Chem.* **2021**, *5* (12), 859−869.
(39) Matyjaszewski, K. Advanced Materials by Atom Transfer Radical Polymerization. *Adv. Mater.* **2018**, *30* (23), 1706441.
(40) Georgopanos, P.; Lo, T. Y.; Ho, R. M.; Avgeropoulos, A. Synthesis, Molecular Characterization and Self-Assembly of (PS-*b*-PDMS)$_n$ Type Linear (n = 1, 2) and Star (n = 3, 4) Block Copolymers. *Polym. Chem.* **2017**, *8* (5), 843−850.
(41) Fragiadakis, D.; Pissis, P.; Bokobza, L. Glass Transition and Molecular Dynamics in Poly(dimethylsiloxane)/Silica Nanocomposites. *Polymer* **2005**, *46* (16), 6001−6008.
(42) Petr, M.; Katzman, B.; DiNatale, W.; Hammond, P. T. Synthesis of a New, Low-T_g Siloxane Thermoplastic Elastomer with a Functionalizable Backbone and Its Use as a Rapid, Room Temperature Photoactuator. *Macromolecules* **2013**, *46* (7), 2823−2832.
(43) Mai, Y.; Eisenberg, A. Self-Assembly of Block Copolymers. *Chem. Soc. Rev.* **2012**, *41* (18), 5969.
(44) Zhang, J.; Zhou, P.; Shi, B.; Li, P.; Wang, G. High-Efficient Access to Inverse Morphologies via Living Anionic Polymerization-Mediated Polymerization-Induced Cooperative Assembly. *Macromolecules* **2023**, *56* (15), 5743−5753.
(45) Zhou, P.; Shi, B.; Liu, Y.; Li, P.; Wang, G. Exploration of the Modification-Induced Self-Assembly (MISA) Technique and the Preparation of Nano-Objects with a Functional Poly(acrylic acid) Core. *Polym. Chem.* **2022**, *13* (28), 4186−4197.
(46) Chai, X.; Zhou, P.; Xia, Q.; Shi, B.; Wang, G. Fluorine-Containing Nano-Objects with the Same Compositions but Different Segment Distributions: Synthesis, Characterization and Comparison. *Polym. Chem.* **2022**, *13* (45), 6293−6301.
(47) Zhang, Q.; Hoogenboom, R. Polymers with Upper Critical Solution Temperature Behavior in Alcohol/Water Solvent Mixtures. *Prog. Polym. Sci.* **2015**, *48*, 122−142.
(48) Cowie, J. M. G.; Mohsin, M. A.; McEwen, I. J. Alcohol-Water Cosolvent Systems for Poly(methyl methacrylate). *Polymer* **1987**, *28* (9), 1569−1572.
(49) Barton, A. F. M. *CRC Handbook of Solubility Parameters and Other Cohesion Parameters*; Routledge: New York, 2017.
(50) Vandenburg, H. J.; Clifford, A. A.; Bartle, K. D.; Carlson, R. E.; Carroll, J.; Newton, I. D. A Simple Solvent Selection Method for Accelerated Solvent Extraction of Additives from Polymers. *Analyst* **1999**, *124* (11), 1707−1710.
(51) Lee, J. N.; Park, C.; Whitesides, G. M. Solvent Compatibility of Poly(dimethylsiloxane)-Based Microfluidic Devices. *Anal. Chem.* **2003**, *75* (23), 6544−6554.
(52) Yang, J.; Chen, A.; Liu, F.; Gu, L.; Xie, X.; Ding, Z. Hybrid Coating of Polydimethylsiloxane with Nano-ZrO_2 on Magnesium Alloy for Superior Corrosion Resistance. *Ceram. Int.* **2022**, *48* (23), 35280−35289.
(53) Gui, Y.; Sun, S. L.; Han, Y.; Zhang, H. X.; Zhang, B. Y. Influence of the Rubber Crosslinking Density of a Core-Shell Structure Modifier on the Properties of Toughened Poly(methyl methacrylate). *J. Appl. Polym. Sci.* **2010**, *115* (4), 2386−2393.
(54) Wrotecki, C.; Heim, P.; Gaillard, P. Rubber Toughening of Poly(methyl methacrylate).1. Effect of the Size and Hard Layer Composition of the Rubber Particles. *Polym. Eng. Sci.* **1991**, *31* (4), 213−217.
(55) Poomalai, P.; Ramaraj, B.; Siddaramaiah. Poly(methyl methacrylate) Toughened by Ethylene-vinyl Acetate Copolymer: Physico-mechanical, Thermal, and Chemical Properties. *J. Appl. Polym. Sci.* **2007**, *104* (5), 3145−3150.
(56) Poomalai, P.; Varghese, T. O.; Siddaramaiah. Investigation on Thermoplastic Co-poly(ether-ester) Elastomer Toughened Poly(methylmethacrylate) Blends. *J. Appl. Polym. Sci.* **2008**, *109* (6), 3511−3518.
(57) Zhang, Y.; Liu, W.; Huang, W.; Ding, Y.; Song, L.; Zheng, S.; Wang, Z. The Toughening of Polymeric Glasses Using Cellulose without Sacrificing Transparency. *Ind. Crops Prod.* **2019**, *142*, 111842.
(58) Poomalai, P.; Varghese, T. O.; Siddaramaiah. Ethylene Methacrylate (EMA) Co-Polymer Toughened Polymethyl Methacrylate Blends: Physico-Mechanical, Optical, Thermal and Chemical Properties. *Polym. Plast. Technol. Eng.* **2009**, *48* (9), 958−965.
(59) Rahman, S. S.; Mahmud, M. B.; Monfared, A. R.; Lee, P. C.; Park, C. B. Achieving Outstanding Toughness of PMMA While Retaining Its Strength, Stiffness, and Transparency Using in Situ Developed TPEE Nanofibrils. *Compos. Sci. Technol.* **2023**, *236*, 109994.
(60) Wang, W.; Liang, T.; Zhang, B.; Bai, H.; Ma, P.; Dong, W. Green Functionalization of Cellulose Nanocrystals for Application in Reinforced Poly(methyl methacrylate) Nanocomposites. *Carbohydr. Polym.* **2018**, *202*, 591−599.
(61) Dong, H.; Sliozberg, Y. R.; Snyder, J. F.; Steele, J.; Chantawansri, T. L.; Orlicki, J. A.; Walck, S. D.; Reiner, R. S.; Rudie, A. W. Highly Transparent and Toughened Poly(methyl methacrylate) Nanocomposite Films Containing Networks of Cellulose Nanofibrils. *ACS Appl. Mater. Interfaces* **2015**, *7* (45), 25464−25472.
(62) Song, S.; Li, Q.; Zhang, C.; Liu, Z.; Fan, X.; Zhang, Y. Balanced Strength-Toughness, Thermal Conductivity and Self-Cleaning Properties of PMMA Composites Enabled by Terpolymer Grafted Carbon Nanotube. *Nanotechnology* **2021**, *32* (19), 195709.
(63) Yihun, F. A.; Ifuku, S.; Saimoto, H.; Izawa, H.; Morimoto, M. Highly Transparent and Flexible Surface Modified Chitin Nanofibers Reinforced Poly(methyl methacrylate) Nanocomposites: Mechanical, Thermal and Optical Studies. *Polymer* **2020**, *197*, 122497.
(64) Guan, Q.; Lu, X.; Chen, Y.; Zhang, H.; Zheng, Y.; Neisiany, R. E.; You, Z. High-performance Liquid Crystalline Polymer for Intrinsic Fire-resistant and Flexible Triboelectric Nanogenerators. *Adv. Mater.* **2022**, *34* (34), 2204543.
(65) Li, L.; Liu, X.; Wang, J.; Yang, Y.; Cao, Y.; Wang, W. New Application of MXene in Polymer Composites toward Remarkable Anti-Dripping Performance for Flame Retardancy. *Composites, Part A* **2019**, *127*, 105649.
(66) Zhan, J.; Wang, L.; Hong, N.; Hu, W.; Wang, J.; Song, L.; Hu, Y. Flame-Retardant and Anti-Dripping Properties of Intumescent Flame-Retardant Polylactide with Different Synergists. *Polym. Plast. Technol. Eng.* **2014**, *53* (4), 387−394.
(67) Yin, Y.; Li, W.; Feng, M.; Hu, X.; Niu, J.; Yao, J. Fabrication of Flame-Retardant and Anti-Dripping Waterborne Polyurethane Containing Phosphorus/Silicon via a Green and Feasible Strategy. *ACS Sustain. Chem. Eng.* **2025**, *13* (9), 3522−3533.

https://doi.org/10.1021/acsapm.5c04232
ACS Appl. Polym. Mater. 2026, 8, 2731−2745